JOURNAL OF SPACECRAFT AND ROCKETS
Vol. 36, No. 5, September–October 1999

High-Supersonic/Hypersonic Flutter of Prismatic Composite Plate/Shell Panels

S. Wang*
Loughborough University, Loughborough, England LE11 3TU, United Kingdom

A spline finite strip modal method is developed for flutter instability analysis of prismatic composite plate/shell panels exposed to high-supersonic/hypersonic flow. The structural model is formulated within the context of first-order shear deformation shell theory, and the aerodynamic pressure is evaluated using the two-dimensional static aerodynamic approximation. The thermal effect due to aerodynamic heating is not considered. The analysis consists of two stages. In the first stage, the free-vibration problem of the panel is performed by using a superstrip concept and a multilevel substructuring technique. The natural frequencies and vibration modes are, thus, obtained by employing the highly reliable bisection Sturm sequence approach with great accuracy and efficiency. In the second stage, the obtained natural frequencies and the corresponding mode shapes are utilized to reduce considerably the size of the original aeroelastic eigenvalue problem, which is then solved to determine the critical dynamic pressure and the corresponding flutter frequency. A variety of numerical experiments, which are conducted to validate and test the performance of the formulation, demonstrates the reliability, efficiency, accuracy, and versatility of the method.

Nomenclature

A = structure length
$\boldsymbol{A}$ = eigenvector
B = structure width
b = finite strip width
c = superstrip order
D = bending rigidity
$\boldsymbol{D}$ = structure nodal displacement vector
$\boldsymbol{d}$ = strip nodal displacement vector
E, E_L, E_T = lamina Young's modulus
$\boldsymbol{e}$ = laminate strain and curvature vector
$\boldsymbol{F}$ = laminate stress resultant vector
G_{LT}, G_{TT} = lamina shear modulus
h = laminate thickness
$\boldsymbol{K}$ = structure stiffness matrix
$\boldsymbol{K}_a$ = structure aerodynamic stiffness matrix
k = spline function order
$\boldsymbol{k}$ = finite strip stiffness matrix
$\boldsymbol{k}_a$ = finite strip aerodynamic stiffness matrix
$\boldsymbol{L}$ = laminate constitutive matrix
M = Mach number
$\boldsymbol{M}$ = structure mass matrix
m = number of modes
$\boldsymbol{m}$ = finite strip mass matrix
N_i = Lagrangian shape function
$\boldsymbol{N}_i$ = Lagrangian shape function matrix
n = Lagrangian shape function order
$\boldsymbol{Q}$ = lamina constitutive matrix
q = number of spline sections
q_0 = dynamic pressure
R = radius
$\boldsymbol{S}$ = diagonal matrix of spline function bases
T = kinetic energy
U = strain energy
u = midsurface displacement along the x axis
v = midsurface displacement along the y axis
W = virtual work of aerodynamic pressure
w = displacement along the z axis
x, y, z = coordinates
Δp = aerodynamic pressure
$\boldsymbol{\delta}$ = displacement vector
$\boldsymbol{\varepsilon}$ = lamina strain vector
$\boldsymbol{\eta}$ = modal coordinate vector
λ = dynamic pressure parameter
$\lambda_{\rm cr}$ = critical dynamic pressure parameter
$\lambda^*_{\rm cr}$ = nondimensional critical dynamic pressure parameter
ν, ν_{LT} = material Poisson's ratio
ρ = material density
$\boldsymbol{\sigma}$ = lamina stress vector
$\bar{\boldsymbol{\Phi}}$ = modified B-spline function base
$\boldsymbol{\Psi}$ = modal matrix
ψ_x = midsurface normal rotation along the x axis
ψ_y = midsurface normal rotation along the y axis
$\boldsymbol{\Omega}$ = diagonal matrix of natural frequencies
ω = natural frequency
$\omega_{\rm cr}$ = flutter frequency
$\omega^*_{\rm cr}$ = nondimensional flutter frequency parameter

Received 1 May 1998; revision received 21 October 1998; accepted for publication 24 October 1998.

*Lecturer, Department of Aeronautical and Automotive Engineering. Member AIAA.

Introduction

PLATE/SHELL panels are major load carrying structural components of manufactured flying vehicles such as aircrafts, space stations, missiles, aerospace launching vehicles, etc. Reflecting humankind's ever-lasting endeavor to fly fast, high, and yet with marvellous acrobatic agility, more and more these panels are being constructed using advanced fiber-reinforced composite materials to achieve minimum weight design. Apart from possessing high specific stiffness and high specific strength, these materials offer structure design engineers a wonderful tailoring package including, particularly, the fiber orientation and lamination scheme to ascertain a structure design with maximum efficiency. For very apparent reasons, these materials may be the best candidate for use in the design of flying vehicles at high-supersonic/hypersonic speed. There is, thus, a great need to investigate the aerodynamic behavior of these composite plate/shell panels. One important such behavior is the high-supersonic/hypersonic flutter occurring due to the interaction between the elastic deformation of the panel and the aerodynamic pressure. By taking the advantage of the geometry of the prismatic panels, this paper develops a spline finite strip modal method to predict the critical dynamic pressure and the corresponding flutter frequency of these panels in a high-supersonic/hypersonic airflow. The method underpins the four crucial aspects of a prediction: reliability, efficiency, accuracy, and versatility.

Although it is not as notorious as the conventional lifting surface or wing flutter that has brought many catastrophic failures,

panel flutter instability can induce various failure mechanisms. At least two are readily identifiable and have occurred in practice. If the flutter-induced stress state exceeds the material failure criterion, then catastrophic or rapid structural collapse occurs; on the other hand, if the stress amplitudes are relatively small, then structural fatigue failure may occur. These detrimental consequences have led to extensive research activities on the topic. An early survey on the subject up to 1966 was given by Dugundji.[1] A thorough and definitive summary on the study up to the mid-1970s was presented by Dowell.[2,3] Another valuable monograph on the topic was written by Librescu.[4] In the late 1980s a renewed interest emerged in panel flutter analysis at high-supersonic/hypersonic speed because of the resurgent interest in flight vehicles such as the high-speed civil transport (HSCT), the National Aerospace plane (NASP), and the advanced tactical fighter that will operate at high-supersonic/hypersonic Mach numbers. Reed et al.[5] conducted a survey in the area of hypersonic flutter in support of the NASP program. Most recently, Gray and Mei[6] gave a complete survey on various theoretical considerations and numerical methods for nonlinear panel flutter analysis. These surveys and the literature search conducted by the author have shown that most of the research work in this area is concerned with single plates/shells that may be made of either isotropic materials or fiber-reinforced composite materials. It is noted that Liao and Sun[7] and Lee and Lee[8] have reported flutter investigations of stiffened composite plates and shells. In their studies, the stiffeners are treated as beam elements. It is believed that the present study is the first work to deal with the flutter instability of prismatic composite plate/shell panels of general cross sections.

The present spline finite strip modal method is developed based on an earlier development of a spline finite strip method (FSM) for free-vibration and static buckling analyses of prismatic composite plate/shell structures.[9,10] The purpose of the development is to combine the powerful multilevel substructuring technique used in the FSM[9,10] and the efficient modal method and, thus, to provide a fast analysis capability for predicting the critical dynamic pressure and flutter frequency of prismatic composite plate/shell panels of complicated cross sections. The theoretical formulation of the method is established, and a variety of numerical experiments are conducted to demonstrate the capability of the formulation.

Theoretical Formulations

Spline Finite Strip Model

A single curved plate strip, which is assumed to form part of a prismatic plate/shell structure, is shown in Fig. 1. The finite strip has uniform radius of curvature R, which is infinite for a flat plate strip, uniform thickness h, and curved breadth b. The strip spans the whole length of the structure, which is A. The local axes xyz are surface ones, i.e., are axial (or longitudinal), tangential (or circumferential), and normal ones. The translational displacements at a general point in the direction of the surface axes are $\bar{u}$, $\bar{v}$, and $\bar{w}$, and at a point on the middle surface are u, v, and w. The total rotations of the middle-surface normal along the x and y directions are ψ_x and ψ_y.

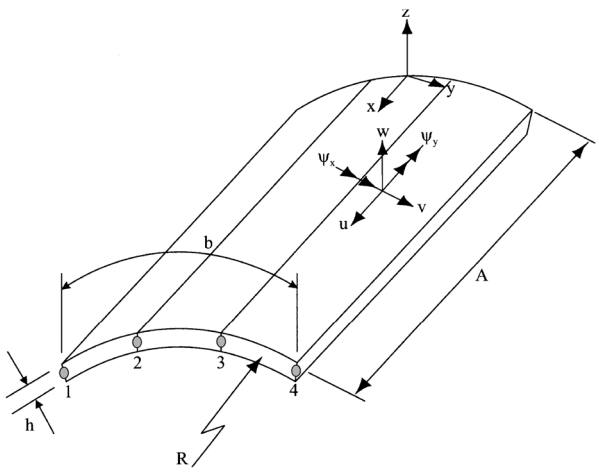

Fig. 1 Curved finite strip.

The basic assumption for displacement behavior in first-order shear deformation shell theory (SDST) is of the form

$$\begin{aligned}\bar{u}(x, y, z, t) &= u(x, y, t) + z\psi_x(x, y, t)\\ \bar{v}(x, y, z, t) &= v(x, y, t) + z\psi_y(x, y, t)\\ \bar{w}(x, y, z, t) &= w(x, y, t)\end{aligned} \tag{1}$$

where t is the time dimension. Thus, the displacement at a general point in the structure is expressed in terms of five fundamental middle-surface quantities, namely, u, v, w, ψ_x, and ψ_y.

The linear expressions for the five significant strain components of the enhanced Koiter-Sanders SDST[11,12] are, at a general point,

$$\begin{Bmatrix}\varepsilon_x\\ \varepsilon_y\\ \gamma_{yz}\\ \gamma_{xz}\\ \gamma_{xy}\end{Bmatrix} = \begin{Bmatrix}u_{,x} + z\psi_{x,x}\\ v_{,y} + w/R + z\psi_{y,y}\\ w_{,y} + \psi_y - v/R\\ w_{,x} + \psi_x\\ u_{,y} + v_{,x} + z(\psi_{x,y} + \psi_{y,x} + [v_{,x} - u_{,y}]/2R)\end{Bmatrix} \tag{2}$$

Here ε_x and ε_y are in-surface direct strains, γ_{xy} is the in-surface engineering shear strain, and γ_{yz} and γ_{zx} are the through-thickness shear strains.

In general, the finite strip is assumed to be a laminate, which is composed of a number of bonded layers of unidirectional fiber-reinforced composite material. Making the usual assumptions, the stress–strain relationships at a general point for a layer are

$$\boldsymbol{\sigma} = \boldsymbol{Q}\boldsymbol{\varepsilon} \tag{3}$$

where

$$\boldsymbol{\sigma} = (\sigma_x, \sigma_y, \tau_{yz}, \tau_{zx}, \tau_{xy})^T \tag{4}$$

$$\boldsymbol{\varepsilon} = (\varepsilon_x, \varepsilon_y, \gamma_{yz}, \gamma_{zx}, \gamma_{xy})^T \tag{5}$$

$$\boldsymbol{Q} = \begin{bmatrix} Q_{11} & & & & \\ Q_{12} & Q_{22} & \text{symmetric} & & \\ 0 & 0 & Q_{44} & & \\ 0 & 0 & Q_{45} & Q_{55} & \\ Q_{16} & Q_{26} & 0 & 0 & Q_{66}\end{bmatrix} \tag{6}$$

In Eq. (6), Q_{ij} for $i, j = 1, 2, 6$, are plane-stress reduced stiffness coefficients, and Q_{ij} for $i, j = 4, 5$, are through-thickness shear stiffness coefficients.

The constitutive equations for the laminate are obtained through use of Eqs. (2) and (3) and appropriate integration through the thickness. They are

$$\boldsymbol{F} = \boldsymbol{L}\boldsymbol{e} \tag{7}$$

where

$$\boldsymbol{F} = (N_x, N_y, N_{xy}, M_x, M_y, M_{xy}, Q_y, Q_x)^T \tag{8}$$

$$\begin{aligned}\boldsymbol{e} = (&u_{,x}, v_{,y} + w/R, u_{,y} + v_{,x}, \psi_{x,x}, \psi_{y,y}, \psi_{x,y} + \psi_{y,x}\\ &+ [v_{,x} - u_{,y}]/2R, w_{,y} + \psi_y - v/R, w_{,x} + \psi_x)^T\end{aligned} \tag{9}$$

$$\boldsymbol{L} = \begin{bmatrix} A_{11} & & & & & & & \\ A_{12} & A_{22} & & \text{symmetric} & & & & \\ A_{16} & A_{26} & A_{66} & & & & & \\ B_{11} & B_{12} & B_{16} & D_{11} & & & & \\ B_{12} & B_{22} & B_{26} & D_{12} & D_{22} & & & \\ B_{16} & B_{26} & B_{66} & D_{16} & D_{26} & D_{66} & & \\ 0 & 0 & 0 & 0 & 0 & 0 & A_{44} & \\ 0 & 0 & 0 & 0 & 0 & 0 & A_{45} & A_{55}\end{bmatrix} \tag{10}$$

Here N_x, N_y, and N_{xy} are the membrane direct and shearing forces per unit length; M_x, M_y, and M_{xy} are the bending and twisting

moments per unit length; and Q_x and Q_y are the through-thickness shear forces per unit length. The laminate stiffness coefficients are defined as

$$(A_{ij}, B_{ij}, D_{ij}) = \int_{-h/2}^{h/2} Q_{ij}(1, z, z^2)\,\mathrm{d}z, \qquad i, j = 1, 2, 6 \tag{11}$$

$$A_{ij} = k_i k_j \int_{-h/2}^{h/2} Q_{ij}\,\mathrm{d}z, \qquad i, j = 4, 5 \tag{12}$$

The parameters $k_i k_j$ are the prescribed shear correction factors, introduced to allow for the through-thickness shear strain distributions not being uniform through the laminate thickness. In this study, these shear correction factors are taken to be $\frac{5}{6}$.

The form of the constitutive Eq. (7) assumed here is very general. It allows for anisotropic laminate properties with regard to both in-surface and out-of-surface behaviors, for full coupling between in-surface and out-of-surface behavior, and for through-thickness shearing action.

The strain energy of the curved strip is

$$U = \frac{1}{2}\int_V \boldsymbol{\sigma}^T \boldsymbol{\varepsilon}\,\mathrm{d}V = \frac{1}{2}\int_V \boldsymbol{\varepsilon}^T \boldsymbol{Q}\boldsymbol{\varepsilon}\,\mathrm{d}V \tag{13}$$

where V denotes the volume of the strip. With the definitions given earlier, U can also be expressed as

$$U = \frac{1}{2}\int_{-b/2}^{b/2}\int_0^A \boldsymbol{e}^T \boldsymbol{L}\boldsymbol{e}\,\mathrm{d}x\,\mathrm{d}y \tag{14}$$

with $\boldsymbol{e}$ and $\boldsymbol{L}$ defined in Eqs. (9) and (10), respectively. The expanded form of Eq. (14), with the triple matrix product evaluated, becomes

$$\begin{aligned}
U = \frac{1}{2}\int_{-b/2}^{b/2}\int_0^A \Bigg(& A_{11}u_{,x}^2 + A_{22}\left(v_{,y} + \frac{w}{R}\right)^2 + A_{66}(v_{,x} + u_{,y})^2 \\
& + 2A_{12}u_{,x}\left(v_{,y} + \frac{w}{R}\right) + 2A_{16}u_{,x}(u_{,y} + v_{,x}) \\
& + 2A_{26}\left(v_{,y} + \frac{w}{R}\right)(u_{,y} + v_{,x}) + 2B_{11}u_{,x}\psi_{x,x} \\
& + 2B_{22}\left(v_{,y} + \frac{w}{R}\right)\psi_{y,y} + 2B_{66}(u_{,y} + v_{,x})\left[\psi_{x,y} + \psi_{y,x}\right. \\
& \left. + \frac{(v_{,x} - u_{,y})}{2R}\right] + 2B_{12}\left[u_{,x}\psi_{y,y} + \left(v_{,y} + \frac{w}{R}\right)\psi_{x,x}\right] \\
& + 2B_{16}\left\{u_{,x}\left[\psi_{x,y} + \psi_{y,x} + \frac{(v_{,x} - u_{,y})}{2R}\right] + \psi_{x,x}[u_{,y} + v_{,x}]\right\} \\
& + 2B_{26}\left\{v_{,y}\left[\psi_{x,y} + \psi_{y,x} + \frac{(v_{,x} - u_{,y})}{2R}\right] + \psi_{y,y}[u_{,y} + v_{,x}]\right\} \\
& + D_{11}\psi_{x,x}^2 + D_{22}\psi_{y,y}^2 + D_{66}\left[\psi_{x,y} + \psi_{y,x} + \frac{(v_{,x} - u_{,y})}{2R}\right]^2 \\
& + 2D_{12}\psi_{x,x}\psi_{y,y} + 2D_{16}\psi_{x,x}\left[\psi_{x,y} + \psi_{y,x} + \frac{(v_{,x} - u_{,y})}{2R}\right] \\
& + 2D_{26}\psi_{y,y}\left[\psi_{x,y} + \psi_{y,x} + \frac{(v_{,x} - u_{,y})}{2R}\right] \\
& + A_{44}\left(w_{,y} + \psi_y - \frac{v}{R}\right)^2 + A_{55}(w_{,x} + \psi_x)^2 \\
& + 2A_{45}(\psi_x + w_{,x})\left(\psi_y + w_{,y} - \frac{v}{R}\right)\Bigg)\,\mathrm{d}x\,\mathrm{d}y
\end{aligned} \tag{15}$$

It is seen that the highest-order derivatives occurring in this strain energy expression are first derivatives and, hence, only C^0-type continuity is required for the five fundamental quantities. It is noted that when $1/R = 0$ the preceding development reduces to that of the shear deformation plate theory.

The kinetic energy of the strip is

$$T = \frac{1}{2}\int_{-b/2}^{b/2}\int_0^A \rho h\left(\dot{u}^2 + \dot{v}^2 + \dot{w}^2 + \frac{h^2}{12}\left[\dot{\psi}_x^2 + \dot{\psi}_y^2\right]\right)\mathrm{d}x\,\mathrm{d}y \tag{16}$$

on the assumption made here that the mass density ρ is uniform throughout the volume of the strip.

When the strip is a part of the main skin of the panel, which is exposed to the high-supersonic/hypersonic airflow, the disturbed aerodynamic pressure exerted on it is evaluated using the two-dimensional static aerodynamic theory,[13] namely,

$$\Delta p(x, y) = \lambda w_{,x} \tag{17}$$

In Eq. (17) λ is a dynamic pressure parameter defined as

$$\lambda = \frac{2q_0}{(M^2 - 1)^{\frac{1}{2}}} \tag{18}$$

where q_0 is the dynamic pressure and M the Mach number. It is assumed that the airflow is in the x direction, i.e., the strip direction. The virtual work of the aerodynamic pressure is then calculated as

$$W = \int_{-b/2}^{b/2}\int_0^A \lambda w_{,x} w\,\mathrm{d}x\,\mathrm{d}y \tag{19}$$

The strip displacement field is defined by the five fundamental quantities u, v, w, ψ_x, and ψ_y, each of which is assumed to be represented as a summation of products of B-spline functions in the longitudinal x direction and polynomial functions in the circumferential or crosswise y direction. The complete form of the displacement field is

$$\boldsymbol{\delta} = \sum_{i=1}^{n+1} \boldsymbol{N}_i \boldsymbol{S}\boldsymbol{d}_i \tag{20}$$

where

$$\boldsymbol{\delta} = (u, v, w, \psi_y, \psi_x)^T \tag{21}$$

$$\boldsymbol{d}_i = (\boldsymbol{d}^u, \boldsymbol{d}^v, \boldsymbol{d}^w, \boldsymbol{d}^{\psi_y}, \boldsymbol{d}^{\psi_x})_i^T \tag{22}$$

and $\boldsymbol{N}_i$ is a diagonal matrix with all of the diagonal elements being N_i; $\boldsymbol{S}$ is also a diagonal matrix with $\bar{\bar{\boldsymbol{\Phi}}}_k$ as its diagonal elements for u, v, w, and ψ_y, and $\bar{\bar{\boldsymbol{\Phi}}}_{k-1}$ for ψ_x.

In Eq. (20), the quantity i denotes the number of a reference line (at which degrees of freedom are located), and there are $(n+1)$ reference lines for a finite strip, where n is the order of the polynomial representation of each of the fundamental quantities in the crosswise y direction. The N_i are the Lagrangian shape functions that define this polynomial representation for various values of n. The finite strip shown in Fig. 1 corresponds to $n = 3$, i.e., cubic polynomial representation across the strip. The $\boldsymbol{d}^u$, $\boldsymbol{d}^v$, $\boldsymbol{d}^w$, $\boldsymbol{d}^{\psi_y}$, and $\boldsymbol{d}^{\psi_x}$ are time-dependent column matrices of values of generalized displacement parameters at the reference lines relating to u, v, w, ψ_y, and ψ_x, respectively. Also in Eq. (20), the $\bar{\bar{\boldsymbol{\Phi}}}_k$ and $\bar{\bar{\boldsymbol{\Phi}}}_{k-1}$ are modified B-spline function bases of polynomial orders k and $k-1$. In employing the spline functions, the length A is divided into q sections, which are taken to be of equal length, with $q+1$ spline knots within the length A and some other knots (required for the prescription of appropriate end conditions) located outside of the length A. It is noted that Eq. (20) indicates that the $B_{k,k-1}$ approach[14] is used, i.e., the spline representation of ψ_x is one order lower than that of w so as to avoid the shear-locking problem that can otherwise occur when analysing thin structures in the context of first-order shear deformation theory.

The displacement field expression (20) has a variety of variations. Choice can be made regarding the variation of the fundamental quantities in both the crosswise and longitudinal directions. In the crosswise direction, the order n of crosswise Lagrangian interpolation can be selected to be 1, 2, 3, 4, or 5, i.e., the strips are referred to as linear, quadratic, cubic, quartic, or quintic strips. In the longitudinal direction, with the $B_{k,k-1}$ approach, values of k can be selected to be 2, 3, 4, or 5, i.e., the choice lies between B_{21}-, B_{32}-, B_{43}-, and B_{54}-spline representations, as in Ref. 14. Because spline functions possess the flexibility of normal polynomials as well as the efficiency of analytical functions, the spline finite strip method is versatile to deal with any boundary conditions and changes in geometries, loadings, and material properties.

By substituting the displacement field expression (20) into the energy expressions (15) and(16) and the virtual work expression (19), and applying the Hamilton's principle, the aeroelastic equation of motion for the strip is obtained as

$$\boldsymbol{m}\ddot{\boldsymbol{d}} + (\boldsymbol{k} + \lambda \boldsymbol{k}_a)\boldsymbol{d} = \boldsymbol{0} \tag{23}$$

where the $\boldsymbol{m}$, $\boldsymbol{k}$, and $\boldsymbol{k}_a$ are the strip mass, elastic stiffness, and aerodynamic stiffness matrices, respectively, and the $\ddot{\boldsymbol{d}}$, and $\boldsymbol{d}$ are the generalized acceleration and displacement vectors, respectively. The matrices $\boldsymbol{m}$ and $\boldsymbol{k}$ are symmetric, whereas the matrix $\boldsymbol{k}_a$ is skew symmetric. The details of these matrices and vectors are not given here.

Structural Equation and Modal Method

The aeroelastic equation of motion for a structure can be obtained by assembling the matrices $\boldsymbol{m}$, $\boldsymbol{k}$, and $\boldsymbol{k}_a$ in Eq. (23) when they have been transformed into a global coordinate system. Symbolically, it can be expressed as

$$\boldsymbol{M}\ddot{\boldsymbol{D}} + (\boldsymbol{K} + \lambda \boldsymbol{K}_a)\boldsymbol{D} = \boldsymbol{0} \tag{24}$$

By assuming harmonic time-dependence of the motion, i.e.,

$$\boldsymbol{D} = \boldsymbol{A}e^{i\omega t} \tag{25}$$

Eq. (24) becomes

$$\left(\boldsymbol{K} + \lambda \boldsymbol{K}_a - \omega^2 \boldsymbol{M}\right)\boldsymbol{A} = \boldsymbol{0} \tag{26}$$

Equation (26) represents an eigenvalue problem where the eigenvalue is given by ω for a given value of the dynamic pressure parameter λ. When $\lambda = 0$ (corresponding to zero flow velocity), ω is real and represents the natural frequency of the structure. However, as λ increases from zero, the influence of the aerodynamic stiffness matrix $\boldsymbol{K}_a$ will change the nature of the eigenvalue problem. Usually, two real eigenvalues will approach each other and become complex conjugates at a value of $\lambda = \lambda_{\text{cr}}$. This coalescence of modes leads to unbounded motions, and flutter instability occurs. Thus, λ_{cr} is termed as critical dynamic pressure parameter, and the corresponding flutter frequency is ω_{cr}. By employing the QR eigenvalue solver, Eq. (26) can be solved iteratively to yield λ_{cr} and ω_{cr}. For single plates/shells, this direct approach may not present much difficulty because the size of Eq. (26) is relatively small. However, in the case of plate/shell structural panels, the size of Eq. (26) will grows rapidly, and the direct approach will be very time consuming. Further, the direct approach takes no advantages of the symmetry of the mass and stiffness matrices $\boldsymbol{M}$ and $\boldsymbol{K}$ due to the asymmetry of the aerodynamic stiffness matrix $\boldsymbol{K}_a$.

To reduce the size of Eq. (26), the modal method, first applied by Rossettos and Tong,[15] is employed. This method consists of two stages. In the first stage, the free-vibration problem corresponding to $\lambda = 0$ in Eq. (26) is considered to obtain the first m natural frequencies and the normalized mode shapes defined as

$$\boldsymbol{\Psi} = \left(\boldsymbol{A}_1^0, \boldsymbol{A}_2^0, \ldots \boldsymbol{A}_m^0\right) \tag{27}$$

where the superscript 0 denotes that these quantities correspond to $\lambda = 0$ in Eq. (26). In the second stage, the mode shapes $\boldsymbol{\Psi}$ are used to approximate the solution of Eq. (26) in the form

$$\boldsymbol{A} = \boldsymbol{\Psi}\boldsymbol{\eta} \tag{28}$$

where $\boldsymbol{\eta}$ is the vector of generalized modal coordinates. Then using Eq. (28) and premultiplying by $\boldsymbol{\Psi}^T$ reduces Eq. (26) to

$$\left(\boldsymbol{\Omega}^2 + \lambda \boldsymbol{\Psi}^T \boldsymbol{K}_a \boldsymbol{\Psi}\right)\boldsymbol{\eta} = \omega^2 \boldsymbol{\eta} \tag{29}$$

where $\boldsymbol{\Omega}^2$ is a diagonal matrix with the squares of the structural natural frequencies as its elements. The size of the eigenvalue problem Eq. (29) is $m \times m$ and, in general, is much smaller than the size of Eq. (26) and can be easily solved using the QR method.

The efficiency of this modal method depends heavily on the first stage. The powerful superstrip concept and multilevel substructuring technique described in Refs. 9 and 10 are extended to determine the natural frequencies and the mode shapes. Typically, each component curved or flat plate of a structure is represented by one superstrip, which is created as an assembly of 2^c identical strips (where $c = 0$, 1, 2, ...) by an efficient repetitive substructuring procedure. The assembly of 2^c strips is called a superstrip of order c, or simply a superstripC. The superstrip has degrees of freedom located only at its outside edges and where c is chosen to have the value three, for example (as is typical), is a very accurate model of crosswise structural behavior. Usually a prismatic structure is modeled as an assembly of superstrips with a rotation transformation applied as necessary to each edge of the superstrip to transform properties to a general coordinate system. An eccentricity transformation may also be applied if deemed to be of significance. Beyond the superstrip level, higher levels of substructuring can often be invoked, where the structure has a repetitive nature, and this helps further in reducing the number of effective degrees of freedom. The final eigenvalue problem is nonlinear, and determination of the natural frequencies is made using an extended Sturm sequence-bisection approach. Details of this are given in Refs. 9 and 10. Once a specified natural frequency is determined, the mode shapes can be found efficiently by re-entering the hierarchic substructures and superstrips. As a matter of fact, the first stage analysis is embodied in a software package called PASSAS.[10] The package has two versions, corresponding to the use of thin shell theory and of shear deformable shell theory. It provides the means of determining the natural frequencies, buckling stresses, and mode shapes of complicated prismatic structures with general end conditions in an accurate and economical fashion.

Note that the very accurate structural model used in the first stage is also used to generate the aerodynamic stiffness matrix $\boldsymbol{K}_a$ in the second stage. To avoid the large storage requirement of the whole $\boldsymbol{K}_a$, the operation is performed in the individual basic strip level. A bisection iterative QR solver is employed to solve the final eigenvalue Eq. (29) to determine the λ_{cr} and ω_{cr}. Numerical applications are presented in the next section.

Numerical Applications

General Remarks

The objective of the presented numerical applications is to validate the proposed spline finite strip modal method formulated in the preceding section. The applications include single composite plates/shells and composite plate panels of complicated cross sections. Attention here is restricted to the use of only one kind of finite strip model in which $n = 3$ and $k = 3$, i.e., cubic interpolation across a strip and B_{32}-spline representation longitudinally. All of the numerical experiments are conducted in a manner of convergence studies with respect to the number of spline sections q, the order of superstrips c, and the number of modes m. This form of presentation is particularly necessary in flutter instability analysis to have confidence in the converged results because the convergence of the critical dynamic pressure parameter λ_{cr} and the flutter frequency ω_{cr} often do not converge monotonically and have no any upper-bound or lower-bound guidance.

A broad specification of end or edge conditions can be made when using the method but in the applications described here the conditions are those of simple support or of full clamping. They are defined as, for instance, at $x = 0$, simple support: $u \neq 0$, $v = 0$, $w = 0$, $\psi_x \neq 0$; and $\psi_y = 0$; and clamped support: $u = v = w = \psi_x = \psi_y = 0$. In the applications that follow, the present predictions are compared, wherever possible, with results available in the literature.

Single Plates/Shells

The first example is concerned with a thin square isotropic plate, which is simply supported at all the four edges, designated as SSSS. The problem has been considered in Ref. 16 based on classical plate theory. In the present SDST analysis, the thickness-to-length ratio, i.e., h/A, is taken to be 0.001 to ignore the through-thickness shear effects. Predictions for flutter instability are given in Table 1 in terms of a nondimensional dynamic pressure parameter λ^*_{cr} defined as

$$\lambda^*_{cr} = \frac{\lambda_{cr} A^3}{D} \tag{30}$$

and a flutter frequency parameter ω^*_{cr} defined as

$$\omega^*_{cr} = \frac{\omega^2_{cr} \rho h A^4}{D} \tag{31}$$

where $D = Eh^3/12(1-\nu^2)$ and $\nu = 0.3$. The number of modes m used increases from 5 to 40 with an increment of 5, and three different structural modelings, i.e., $q = 4$, $c = 2$; $q = 8$, and $c = 3$; and $q = 16$, $c = 4$, are employed. In each modeling, a single superstrip of order c, i.e., superstripC, is used to model the whole plate. It is observed that the manner of convergence of the predictions is very good, though nonmonotonic characteristics exist. Comparing with the exact values from Ref. 16, Table 1 shows that the structural modeling $q = 8$, $c = 3$ with $m = 25$ can yield very accurate results. It is also noted that the predictions with $m = 10$ are generally in a close agreement with those with $m = 25$. The research work on this problem in Ref. 15 has also concluded that accurate results can be obtained by using only several modes. However, note that the number of modes used to achieve a converged solution is problem dependent. Usually, a large number of modes should be used to determine the critical flutter instability with high reliability. This is especially true when complicated plate/shell panels are considered.

Table 1 Values of λ^*_{cr} and ω^*_{cr} for a thin square isotropic SSSS plate

	λ^*_{cr}			ω^*_{cr}		
m	$q=4$, $c=2$	$q=8$, $c=3$	$q=16$, $c=4$	$q=4$, $c=2$	$q=8$, $c=3$	$q=16$, $c=4$
5	386.657	383.702	383.551	1421.94	1412.88	1412.44
10	513.018	505.259	505.118	1817.69	1822.01	1822.64
15	496.033	505.059	505.118	1778.55	1822.01	1822.64
20	502.612	513.476	513.851	1798.75	1848.28	1849.94
25	502.612	511.706	511.825	1798.75	1844.21	1845.24
30	502.612	511.706	511.826	1798.75	1844.21	1845.24
35	502.612	512.239	512.807	1798.75	1845.86	1848.17
40	502.612	512.239	512.766	1798.75	1845.86	1849.16
Ref. 16 exact value			512.651			1848.21

Table 2 Values of λ^*_{cr} and ω^*_{cr} for a thin square isotropic CCCC plate

	λ^*_{cr}			ω^*_{cr}		
m	$q=4$, $c=2$	$q=8$, $c=3$	$q=16$, $c=4$	$q=4$, $c=2$	$q=8$, $c=3$	$q=16$, $c=4$
5	646.133	695.464	714.335	3431.20	3607.99	3682.24
10	824.488	838.410	838.269	4138.56	4234.82	4235.73
15	824.488	838.482	838.343	4138.56	4282.17	4236.10
20	824.488	852.610	853.244	4138.56	4292.30	4296.57
25	824.488	849.893	850.125	4138.56	4282.85	4285.58
30	824.484	849.883	850.115	4138.55	4282.82	4285.55
35	824.484	850.549	851.296	4138.55	4285.49	4290.28
40	824.484	850.552	851.301	4138.55	4285.50	4290.30
Ref. 16 FEM			850.418			4282.03

Table 3 Values of λ^*_{cr} and ω^*_{cr} for single-composite laminates

	0_6 layers		$[+45/-45/+45]_s$		$[+45/-45]$	
m	λ^*_{cr}	ω^*_{cr}	λ^*_{cr}	ω^*_{cr}	λ^*_{cr}	ω^*_{cr}
5	284.544	884.547	210.343	796.935	100.982	534.098
10	315.903	1170.12	210.868	792.997	132.392	676.275
15	369.044	1143.53	215.041	808.127	140.150	712.017
20	355.703	1114.96	216.897	813.188	140.104	711.835
25	355.703	1114.96	215.900	810.771	137.992	702.428
30	359.004	1124.56	215.994	811.162	137.982	702.401
35	359.004	1124.56	216.299	812.082	137.975	702.376
40	359.004	1124.56	216.291	812.046	138.491	704.739
Ref. 17	359.5		206.5			
Ref. 7					139.259	684.084

Table 1 shows that the structural modeling $q = 8$, $c = 3$ with $m = 25$ can yield very accurate results. It is also noted that the predictions with $m = 10$ are generally in a close agreement with those with $m = 25$. The research work on this problem in Ref. 15 has also concluded that accurate results can be obtained by using only several modes. However, note that the number of modes used to achieve a converged solution is problem dependent. Usually, a large number of modes should be used to determine the critical flutter instability with high reliability. This is especially true when complicated plate/shell panels are considered.

In the next application, the boundary conditions of the plate are changed to be fully clamped and the plate is designated as CCCC. The same analysis is performed, and the results are given in Table 2. Again, convergence is very good, and a close agreement with the comparative solutions [Ref. 16; finite element method (FEM)] is observed.

Next, consideration is given to a group of single composite plates, which includes two simply supported square symmetric laminates with $h/A = 0.001$ and one clamped asymmetric laminate with $h/A = 0.05$. The material properties for the symmetric and asymmetric laminates are $E_L = 100\ \mathrm{GNm}^{-2}$, $E_T = 10\ \mathrm{GNm}^{-2}$, $G_{LT} = G_{TT} = 3.3\ \mathrm{GNm}^{-2}$, $\nu_{LT} = 0.3$, and $E_L = 213.7\ \mathrm{GNm}^{-2}$, $E_T = 18.6\ \mathrm{GNm}^{-2}$, $G_{LT} = G_{TT} = 5.17\ \mathrm{GNm}^{-2}$, $\nu_{LT} = 0.28$, respectively, where L and T represent the direction of fibers and the direction perpendicular to the fibers. It is assumed that all layers in each laminate is of the same thickness. In the analysis, the structural modeling is $q = 8$ and $c = 3$, that is, each laminate is modeled with one superstrip3. The results are shown in Table 3 with convergence studies with respect to the number of modes m, where λ^*_{cr} is defined as

$$\lambda^*_{cr} = \frac{\lambda_{cr} A^3}{D_{11}(0)} \tag{32}$$

for the two symmetric laminates and

$$\lambda^*_{cr} = \frac{\lambda_{cr} A^3}{E_T h^3} \tag{33}$$

for the one asymmetric laminate; ω^*_{cr} is defined as

$$\omega^*_{cr} = \frac{\omega^2_{cr} \rho h A^4}{D_{11}(0)} \tag{34}$$

for the two symmetric laminates and

$$\omega^*_{cr} = \frac{\omega^2_{cr} \rho h A^4}{E_T h^3} \tag{35}$$

for the one asymmetric laminate. The $D_{11}(0)$ in Eqs. (32) and (34) is the value of D_{11} when the fibers are along the x direction. It is seen

Table 5 Values of λ^*_{cr} and ω^*_{cr} for a CCCC isotropic shell: $m = 30$

$q = 8$			$c = 3$		
c	λ^*_{cr}	ω^*_{cr}	q	λ^*_{cr}	ω^*_{cr}
1	856.316	4846.97	4	815.109	4626.52
2	841.514	4775.97	6	838.969	4759.31
3	840.519	4771.59	8	840.519	4771.59
4	840.446	4771.30	10	840.706	4773.48
5	840.440	4771.27	12	840.802	4774.22
Ref. 7	879.620	4821.77		879.620	4821.77

Table 4 Values of λ^*_{cr} and ω^*_{cr} for a CCCC isotropic shell

$q = 8$, $c = 3$									
m:	5	10	15	20	25	30	35	40	45
λ^*_{cr}	620.876	827.948	828.058	843.651	840.521	840.519	840.504	841.285	841.290
ω^*_{cr}	3843.58	4718.56	4719.10	4782.71	4771.59	4771.59	4771.55	4774.70	4774.72

Table 6 Values of λ^*_{cr} and ω^*_{cr} for a CCCC [0/90] laminate shell

	$q = 8, c = 3$								
m:	5	10	15	20	25	30	35	40	45
λ^*_{cr}	154.455	213.428	200.431	202.498	202.502	202.223	202.222	202.222	202.273
ω^*_{cr}	3026.34	3379.69	3312.13	3323.62	3323.64	3322.38	3322.37	3322.37	3322.66

Table 7 Values of λ^*_{cr} and ω^*_{cr} for a CCCC [0/90] laminate shell: $m = 20$

$q = 8$			$c = 3$		
c	λ^*_{cr}	ω^*_{cr}	q	λ^*_{cr}	ω^*_{cr}
1	202.887	3330.61	4	193.469	3242.67
2	202.489	3324.09	6	200.663	3307.73
3	202.498	3323.62	8	202.498	3323.62
4	202.499	3323.60	10	202.863	3326.86
5	202.498	3323.60	12	202.954	3327.75

from Table 3 that the convergence of the results is very satisfactory, and the agreements are generally close with comparative solutions presented at the bottom of Table 3. The maximum difference occurs at the prediction of λ^*_{cr} for the symmetric angle-ply laminate and is about 4.7%. The reason may be due to the violation of natural-boundary conditions of the trigonometric functions used in Ref. 17 for anisotropic laminates.

Now, attention is turned to single shells. First, a clamped isotropic shell is considered. The geometry of the shell is defined as follows: The length is $A = 40$, the midsurface arc breadth is $B = 40$, the thickness is $h = 1$, and the radius is $R = 200$. The Poisson's ratio is $\nu = 0.3$. Again, one single superstrip C is used to model the complete shell. Convergence studies are performed with respect to the number of modes m with $q = 8$ and $c = 3$, to the order of the superstrip c with $q = 8$ and $m = 30$, and to the number of spline sections q with $c = 3$ and $m = 30$. The results are shown in Tables 4 and 5, where λ^*_{cr} and ω^*_{cr} are defined by Eqs. (30) and (31), respectively. It is observed that the convergence with respect to m is nonmonotonic, whereas the convergence with respect to both q and c is monotonic. Further, it is seen that both λ^*_{cr} and ω^*_{cr} converge from the upper side with increase in c, whereas from lower side with increase in q. It is noted that the convergence is excellent. The predictions with $q = 8$, $c = 3$, and $m = 25$ are very close to the finer values and can be regarded as the accurate solutions to the problem. The present predictions of λ^*_{cr} and ω^*_{cr} using this set of parameters are in only 4.4% and 1.0%, respectively, with the comparative solutions. It seems that these differences are due to the inclusion of the aerodynamic damping in Ref. 7.

One clamped laminated composite shell is considered next. The geometry of the shell is defined as follows: The length is $A = 0.254$ m, the midsurface arc breadth is $B = 0.254$ m, the thickness is $h = 0.00254$ m, and the radius is $R = 5.08$ m. The material properties are $E_L = 144.8\ \text{GNm}^{-2}$, $E_T = 9.65\ \text{GNm}^{-2}$, $G_{LT} = 4.14\ \text{GNm}^{-2}$, $G_{TT} = 3.45\ \text{GNm}^{-2}$, $\nu_{LT} = 0.3$, and $\rho = 1575.2\ \text{kgm}^{-3}$. The layup of the shell is [0/90]. The same convergence studies as that for the isotropic shell are performed. Results are presented in Tables 6 and 7, where λ^*_{cr} is defined in Eq. (33), where $\omega^*_{cr} = \omega_{cr}$ (rad/s) is the circular frequency. It is observed from the results that, again, the convergence is nonmonotonic with respect to m, but monotonic with respect to c and q with a little fluctuation of λ^*_{cr}. No comparative solutions are available.

Plate Panels

Numerical applications considered next are concerned with two one-blade-stiffened panels: One is made of isotropic material, and the other made of laminated composite material. The panels are clamped at their two ends and two edges. The two panels have same geometry: The length is $A = 0.15$ m, and the cross section is shown in Fig. 2. The material properties are $E = 69\ \text{GNm}^{-2}$, $\nu = 0.3$, and $\rho = 2670\ \text{kgm}^{-3}$ for the isotropic panel and $E_L = 138\ \text{GNm}^{-2}$, $E_T = 9.7\ \text{GNm}^{-2}$, $G_{LT} = 5.5\ \text{GNm}^{-2}$, $G_{TT} = 4.1\ \text{GNm}^{-2}$, $\nu_{LT} = 0.3$, and $\rho = 1580\ \text{kgm}^{-3}$ for the composite panel. The main plate of the composite panel has 8 layers as

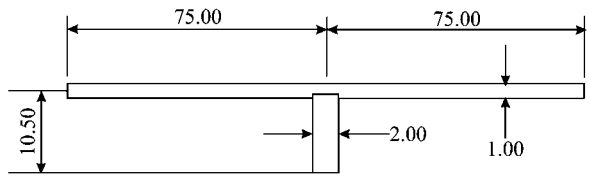

Fig. 2 Cross section of one-blade-stiffened panels (dimensions in millimeters).

$[0/90/0/90]_s$, and the stiffener has 16 layers as $[0/90/0/90]_{2s}$. The thickness of each layer is 0.125 mm. Lee and Lee[8] have recently investigated the flutter instability of these two panels using a finite element modal method. In their study, the main plate is modeled using 8×12 nine-noded elements based on first-order shear deformation plate theory, the stiffener is modeled using eight three-noded Timoshenko beam elements, and 25 modes are employed. Their results are given in graphical form. In the present analysis, the main plate is modeled with two superstrip3, and the stiffener is modeled with one superstrip0. Convergence studies are performed with respect to the number of modes m and the number of spline section q, and they are presented in Table 8, where λ^*_{cr} and ω^*_{cr} are defined in Eqs. (30) and (31) for the isotropic panel and in Eqs. (33) and (35) for the composite panel, with h being the thickness of the main plate. From Table 8 it seen that present predictions of the nondimensional critical dynamic pressure parameter λ^*_{cr} for both panels are in close agreement with those from Ref. 8. The slight difference may arise from the different modelings of the stiffeners. In the present approach, the stiffener is modeled as a two-dimensional plate, whereas in Ref. 8, it is modeled as a Timoshenko beam. The results also demonstrate that the present analysis has a steady and reliable convergence. Highly accurate predictions for flutter instability can be obtained in an efficient way. It is noted that comparative solutions for the critical flutter frequencies are not available.

The final problem considered concerns blade-stiffened and hat-stiffened composite panels referred to as NASA examples 3 and 5, which have been studied by Stroud et al.[18] for buckling analysis. Wang and Dawe[9] have also used these panels to test their spline finite strip formulations for buckling investigations. The panels have a square platform with $A = B = 762$ mm, and their ends and edges are fully clamped. Originally, their ends are diaphragm supported, whereas the edges are simply supported in Ref. 18. The cross section of each panel consists of six repeating elements of width 127 mm, and geometrical details of these are given in Fig. 3 (as are identifying numbers of plate flats).

The panel material is a laminated graphite-epoxy composite with $E_L = 131\ \text{GNm}^{-2}$, $E_T = 13\ \text{GNm}^{-2}$, $G_{LT} = 6.41\ \text{GNm}^{-2}$, $\nu_{LT} = 0.38$, and $\rho = 1600\ \text{kgm}^{-3}$. Component plates are symmetrically laminated in both panels, and all plies are aligned at 0, 90, or ± 45 deg to the longitudinal axis. Full details of the layups, etc., are recorded[18] and are not given here.

In modeling the cross section in the present analysis, each component plate of all six repeating elements is first represented by a superstrip3 because it has been shown in the previous applications that this model gives accurate predictions for flutter instability. Further substructuring is then used to reduce the effective degrees of freedom to those at only seven reference lines, these being the outside edges and the junctions between the six repeating elements of the cross section. The various levels of substructuring, up to and beyond the superstrip level, drastically reduce the number of effective freedoms of the free-vibration problem in the first stage of a flutter analysis. The natural frequencies and mode shapes can be obtained in a very efficient way with absolute certainty and without losing any accuracy. For example, in a structural model with $q = 12$ and $c = 3$,

Table 8 Values of λ^*_{cr} and ω^*_{cr} for two one-blade-stiffened panels

Isotropic panel						Composite panel					
$q = 8$			$m = 25$			$q = 8$			$m = 25$		
m	λ^*_{cr}	ω^*_{cr}	q	λ^*_{cr}	ω^*_{cr}	m	λ^*_{cr}	ω^*_{cr}	q	λ^*_{cr}	ω^*_{cr}
5	1146.92	12296.6	4	1972.56	22048.1	5	526.771	5328.22	4	708.227	6063.73
15	1785.82	15201.3	6	1965.14	16159.0	15	723.320	6164.65	6	732.975	6201.62
25	1950.60	16076.7	8	1950.60	11076.7	25	738.459	6228.45	8	738.459	6228.45
30	1950.72	16077.3	10	1947.21	16056.2	30	738.457	6228.49	10	739.313	6232.88
35	1968.50	16174.8	11	1947.27	16055.9	35	735.361	6216.75	11	739.499	6233.80
40	1968.44	16174.5	12	1947.39	16056.1	40	735.358	6216.74	12	739.621	6234.37
Ref. 8	1928.0			1928.0			717.0			717.0	

Table 9 Values of λ_{cr} (psi) and ω_{cr} (rad/s) for NASA example panels

NASA example 3						NASA example 5					
$q = 12$			$m = 40$			$q = 12$			$m = 40$		
m	λ_{cr}	ω_{cr}	q	λ_{cr}	ω_{cr}	m	λ_{cr}	ω_{cr}	q	λ_{cr}	ω_{cr}
10	2554.75	5401.16	6	406.390	7781.02	10	2894.71	4746.40	6	138.347	9749.51
15	1770.72	5499.90	7	484.811	7772.73	15	1962.27	6347.48	7	96.2031	9716.94
20	1852.10	6747.23	8	506.452	7768.01	20	678.354	7500.64	8	77.7511	9703.04
25	1871.28	6660.92	9	510.966	7764.91	25	691.966	7502.54	9	69.2865	9695.46
30	925.625	7752.81	10	512.727	7762.82	30	324.734	8462.92	10	64.4044	9690.53
35	510.143	7760.25	11	512.849	7761.35	35	58.8049	9684.21	11	61.2003	9686.96
40	512.862	7760.30	12	512.862	7760.30	40	58.8341	9684.23	12	58.8341	9684.23
45	513.725	7759.72	13	512.709	7759.52	45	58.3578	9684.61	13	56.9997	9682.07
50	514.827	7760.30	14	512.622	7758.95	50	59.8020	9685.26	14	55.5127	9680.32

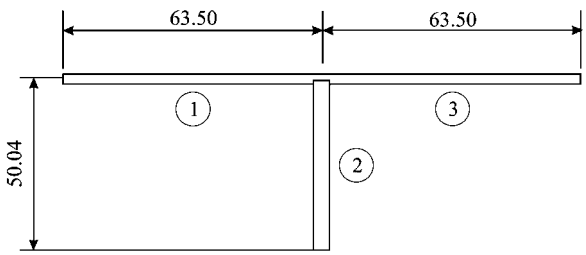

a) Example 3

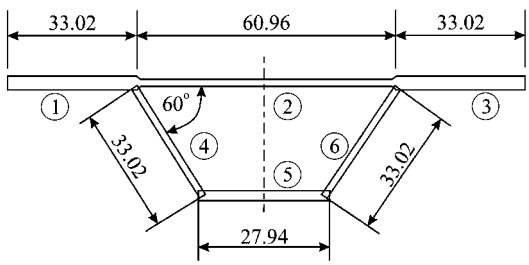

b) Example 5

Fig. 3 Details of the repeating elements (dimensions in millimeters) of NASA example panels.

the obtained natural frequencies and the mode shapes of NASA example 5 panel in this way are exactly the same as those obtained by directly using about over three-quarters of a million degrees of freedom.This greatly reduces the computing cost for a whole flutter analysis. Moreover, the highly accurate natural frequencies and the mode shapes provide a foundation for conducting an accurate flutter analysis. During the second stage, only the main plate of the panels are involved to formulate the aerodynamic stiffness matrix and to perform the modal analysis.Thus, the computing time can be reduced further.

Numerical results are presented in Table 9, and they are the values of the critical dynamic pressure parameter λ_{cr} (pounds per square inch) and the flutter frequency ω_{cr} (radians per second) instead of the nondimensional parameters. For both panels, convergence studies are made against the number of modes m with the number of spline sections q being fixed at 12 and against the q with m being fixed at 40. It is observed that solutions in all cases converge nicely though not in a monotonic manner. One distinctive point noted is that there are sudden big changes in λ_{cr} and ω_{cr} with increase in the number of modes m. For instance, when m changes from 25 to 30, λ_{cr} changes from 1871.28 to 925.625 and ω_{cr} from 6660.92 to 7752.81 for NASA example 3, whereas λ_{cr} changes from 691.966 to 324.734 and ω_{cr} from 7502.54 to 8462.92 for NASA example 5. These changes may indicate changes of coalescent modes. Another interesting point noted is that two close flutter frequencies may correspond to two very different critical dynamic pressures. For instance, in the case of NASA example 3, when $q = 12$ and $m = 30$, the flutter instability corresponds to $\lambda_{cr} = 925.625$ and $\omega_{cr} = 7752.81$, whereas when $q = 12$ and $m = 35$, the flutter instability corresponds to $\lambda_{cr} = 510.143$ and $\omega_{cr} = 7760.25$. It is also noted that the solutions change less dramatically with the changes in the number of spline sections q. Finally, the convergence studies in Table 9 show that the number of modes m used is generally increased to obtain the lowest critical dynamic pressure of prismatic panels of complicated cross section compared with cases of single plates/shells or simple panels. This is reasonable because the coalescence of modes occuring at higher modes is more likely in structures than in single plates/shells. This phenomenon makes the present method of analysis more attractive because it extracts the natural frequencies and mode shape used in the modal analysis in a very economical way.

Conclusions

A spline finite strip modal method is developed for flutter instability analysis of prismatic composite plate/shell panels exposed to high-supersonic/hypersonic flow. First-order shear deformation shell theory is used to formulate the strip properties, and the two-dimensional static aerodynamic theory is used to evaluate the aerodynamic pressure.The novelty of the method is the combination of the powerful multilevel substructuring technique used for free-vibration analysis[9,10] and the efficient modal method.

The method has been applied to a variety of numerical applications, including single composite plates/shells and prismatic composite plate structures. Wherever possible, the present predictions have been compared with existing results, and close agreements have served to validate the method. All of the results are presented in a manner of convergence studies with respect to the number of modes, the number of spline sections, or the order of superstrips. For single plates/shells or simple one-blade-stiffened panels, it shows that accurate predictions can be obtained by using about 20 modes with eight spline sections and superstrip3. Generally, the number

of modes used is increased when panels of complicated cross sections are considered because the coalescence of mode occurs at higher modes, which is more likely in complicated panels than in single plates/shells or simple panels.This makes the present method of analysis more attractive. All of the numerical experiments have demonstrated that the spline finite strip modal method is reliable, efficient, accurate, and versatile.

References

[1]Dugundji,J., "Theoretical Considerations of Panel Flutter at High Supersonic Mach Numbers," *AIAA Journal*, Vol. 4, No. 7, 1966, pp. 1257–1266.

[2]Dowell, E. H., "Panel Flutter: A Review of the Aeroelastic Stability of Plates and Shells," *AIAA Journal*, Vol. 8, No. 3, 1970, pp. 385–399.

[3]Dowell, E. H., *Aeroelasticity of Plates and Shells*, 1st ed., Noordhoff International, Leyden, The Netherlands, 1975, pp. 1–139.

[4]Librescu, L., "Aeroelastic Stability of Anisotropic Multilayered Thin Panels," *Elastostatics and Kinetics of Anisotropic and Heterogeneous Shell-Type Structures*, 1st ed., Noordhoff International, Leyden, The Netherlands, 1975, Chap. 1, pp. 1–281.

[5]Reed, W. H., Hanson, P. W., and Alford, W. J., "Assessment of Flutter Model Testing Relating to the National Aero-Space Plane," NASA CR-1002, July 1987.

[6]Gray, C. E., Jr., and Mei, C., "Large Amplitude Finite Element Flutter Analysis of Composite Panels in Hypersonic Flow," *AIAA Journal*, Vol. 31, No. 6, 1993, pp. 1090–1099.

[7]Liao, C. L., and Sun, Y. W., "Flutter Analysis of Stiffened Laminated Composite Plates and Shells in Supersonic Flow," *AIAA Journal*, Vol. 31, No. 10, 1993, pp. 1897–1905.

[8]Lee, D. M., and Lee, I., "Supersonic Flutter Analysis of Stiffened Isotropic and Anisotropic Panels," *AIAA Journal*, Vol. 34, No. 3, 1996, pp. 637–639.

[9]Wang, S., and Dawe, D. J., "Spline Finite Strip Analysis of the Buckling and Vibration of Composite Prismatic Plate Structures," *International Journal of Mechanical Science*, Vol. 39, No. 10, 1997, pp. 1161–1180.

[10]Dawe, D. J., and Wang, S., "Buckling and Vibration Analysis of Composite Plate and Shell Structures Using the PASSAS Software Package," *Composite Structures*, Vol. 38, No. 1–4, 1997, pp. 541–551.

[11]Koiter, W. T., "A Consistent First Approximation in the General Theory of Thin Elastic Shells," *Theory of Thin Elastic Shells*, edited by W. T. Koiter, North-Holland, Amsterdam, 1960.

[12]Sanders, J. L., "An Improved First-Approximation Theory for Thin Shells," NASA TR-R24, June 1959.

[13]Bisplinghoff, R. L., and Ashley, H., *Principles of Aeroelasticity*, Wiley, New York, 1962, pp. 403–449.

[14]Wang, S., "A Unified Timoshenko Beam B-Spline Rayleigh–Ritz Method for Vibration and Buckling Analysis of Thick and Thin Beams and Plates," *International Journal for Numerical Methods in Engineering*, Vol. 40, No. 3, 1997, pp. 473–491.

[15]Rossettos, J. N., and Tong, P., "Finite Element Analysis of Vibration and Flutter of Cantilever Anisotropic Plates," *Journal of Applied Mechanics*, Vol. 41, Dec. 1974, pp. 1075–1080.

[16]Olson, M. D., "Some Flutter Solutions Using Finite Elements," *AIAA Journal*, Vol. 8, No. 4, 1970, pp. 747–752.

[17]Barai, A., and Durvasula, S., "Flutter of Hybrid Laminated Flat Panels with Simply Supported Edges in Supersonic Flow," *Journal of Sound and Vibration*, Vol. 169, No. 1, 1994, pp. 373–386.

[18]Stroud, W. J., Greene, W. H., and Anderson, M. S., "Buckling Loads of Stiffened Panels Subjected to Combined Longitudinal Compression and Shear: Results Obtained with PASCO, EAL and STAGS Computer Programs," NASA TP2215, Jan. 1984.

R. B. Malla
Associate Editor